Meteorological controls on daily variations of nighttime surface urban heat islands

Jiameng Lai [a], Wenfeng Zhan [a,b,*], James Voogt [c], Jinling Quan [d], Fan Huang [a], Ji Zhou [e], Benjamin Bechtel [f], Leiqiu Hu [g], Kaicun Wang [h], Chang Cao [i], Xuhui Lee [j]

[a] *Jiangsu Provincial Key Laboratory of Geographic Information Science and Technology, International Institute for Earth System Science, Nanjing University, Nanjing, Jiangsu 210023, China*
[b] *Jiangsu Center for Collaborative Innovation in Geographical Information Resource Development and Application, Nanjing 210023, China*
[c] *Department of Geography, University of Western Ontario, London, ON N6A 5C2, Canada*
[d] *State Key Laboratory of Resources and Environmental Information System, Institute of Geographic Sciences and Natural Resources Research, Chinese Academy of Sciences, Beijing 100101, China*
[e] *School of Resources and Environment, University of Electronic Science and Technology of China, Chengdu 611731, China*
[f] *Department of Geography, Ruhr-University Bochum, 44801 Bochum, Germany*
[g] *Department of Atmospheric Science, University of Alabama in Huntsville, AL 35899, USA*
[h] *State Key Laboratory of Earth Surface Processes and Resource Ecology, College of Global Change and Earth System Science, Beijing Normal University, Beijing 100875, China*
[i] *Yale-NUIST Center on Atmospheric Environment, Nanjing University of Information Science and Technology, Nanjing, Jiangsu 210044, China*
[j] *School of Forestry and Environmental Studies, Yale University, New Haven, CT 06511, USA*

ARTICLE INFO

ABSTRACT

Most previous studies of surface urban heat islands (SUHIs) have focused solely on their controlling factors on a seasonal/annual timescale, while the controls on daily variations are largely unknown. By extracting the daily variations of nighttime SUHI features using the Gaussian model and investigating their correlations with various explanatory factors, we have attempted to determine the controls on SUHIs on a daily-basis over Chinese cities. Specific controls of weather conditions on the intensity, extent, shape, and centroid of the SUHIs were identified. Our results show that: (1) SUHI intensity (SUHII) was considerably more sensitive to weather conditions than the SUHI footprint (i.e., extent, shape, and centroid). (2) Meteorological variables including relative humidity, accumulated precipitation, and aerosol optical depth, had the greatest impact on SUHI intensity; whereas factors related to temperature fluctuations (day-to-day fluctuations of surface and air temperature) were the main factors influencing SUHI extent, shape, and the direction in which SUHI centroid varies. (3) Antecedent precipitation substantially impacted the subsequent SUHIs under clear-skies, changing both the SUHI itself and its sensitivity to other factors. Typically, the clear-sky SUHIs directly following rainfall showed a higher dependence on the relative humidity, soil moisture and aerosol, but were less affected by wind. (4) The meteorological contributions to the daily nighttime SUHIIs varied among Chinese cities with different bioclimatic conditions. In general, they were stronger in temperate zones than in subtropical zones. Our results provide an improved understanding of the controls on SUHIs on a daily timescale, as well as a foundation for predicting daily SUHIs based on the influencing meteorological variables.

Acronyms and symbols

Acronyms:

ALB	albedo

(continued on next column)

(continued)

AOD	aerosol optical depth
CUHI	canopy layer urban heat island
CUHII	canopy layer urban heat island intensity

---

* Corresponding authors at: Nanjing University at Xianlin Campus, No. 163, Xianlin Avenue, Qixia District, Nanjing, Jiangsu Province 210023, China.
E-mail addresses: zhanwenfeng@nju.edu.cn (W. Zhan), javoogt@uwo.ca (J. Voogt), quanjl@lreis.ac.cn (J. Quan), jzhou233@uestc.edu.cn (J. Zhou), benjamin.bechtel@rub.de (B. Bechtel), leiqiu.hu@uah.edu (L. Hu), kcwang@bnu.edu.cn (K. Wang), xuhui.lee@yale.edu (X. Lee).

(*continued*)

DL	daytime length
DTR	diurnal temperature range
LST	land surface temperature
NDVI	normalized difference vegetation index
PREP	precipitation
RH	relative humidity
SAT	surface air temperature
SUHI	surface urban heat island
SUHII	surface urban heat island intensity
UHI	urban heat island
WDS	wind speed
Symbols:	
Δ	difference in a quantity over time
φ	SUHI inclination
A	SUHI area
C	SUHI centroid
e	SUHI shape
I	SUHI intensity
p	p value
r	correlation coefficient
T	land surface temperature
Common Subscripts:	
…a	annual average
…d	daily value
…dis	distance
…dir	direction
…mid	mid-term component
…r	rural
…u	urban
…u-r	urban-rural difference
…x	longitudinal (long-axis) direction
…y	latitudinal (short-axis) direction
Δ…a	intra-annual variation
Δ…d	day-to-day variation
Δ…p	averaged magnitude of day-to-day variation (in percentile)

1. Introduction

It is well-known that cities are characterized by significantly elevated temperatures compared to the surrounding rural areas. This phenomenon, commonly known as the urban heat island (UHI) (Oke, 1982), is one of the clearest examples of the anthropogenic modification of climate and can negatively impact both the urban climate and people's lives (Akbari and Konopacki, 2005; Patz et al., 2005).

The UHIs can generally be classified into four types: the boundary-layer UHI, canopy-layer UHI (CUHI), surface UHI (SUHI), and subsurface UHI; of these the CUHI and SUHI have received the most attention (e.g., Chow and Roth, 2006; Haashemi et al., 2016; Hu and Brunsell, 2013; Lai et al., 2018a; Oke, 1982; Peng et al., 2012; Schwarz et al., 2012; Sismanidis et al., 2015; Stewart and Oke, 2012; Tran et al., 2017; Wang et al., 2017; Zhang et al., 2014a). Predicting these two types of UHI are vitally important for improving the quality of urban environments and human life, and a comprehensive understanding of their controlling factors is an indispensable first step (Peng et al., 2018; Zhou et al., 2017). Investigations of the factors controlling the spatiotemporal variations in the CUHI have been extensively documented since 1833 (Arnfield, 2003; Howard, 1833; Oke, 1982), benefiting from the more readily available in-situ measured air temperatures. The factors influencing the SUHI, however, have only been comprehensively investigated in recent decades, once suitable thermal remote sensing data that can depict changes in the large-scale surface thermal status became available (Chakraborty and Lee, 2019; Clinton and Gong, 2013; Huang et al., 2016; Keramitsoglou et al., 2011; Meng et al., 2018; Nichol, 2005; Voogt and Oke, 2003; Wang et al., 2017; Weng, 2009; Zhao et al., 2016; Zhou et al., 2013; Zhou et al., 2015).

The growing availability of remote sensing data has greatly increased satellite-based investigations of the controls on the SUHI (Deilami et al., 2018; Zhou et al., 2019). The results enable us to divide the controls on SUHIs into five groups: (1) land cover types, (2) urban form, (3) anthropogenic heating, (4) climate conditions, and (5) weather conditions. Various studies have confirmed the substantial control of the land cover types (e.g., the vegetation, impervious surface, bare land, water bodies, and buildings) on the spatial variations of the SUHIs over both the pixel and city scales (Chen et al., 2006; Imhoff et al., 2010; Lazzarini et al., 2013; Liu et al., 2017; Mathew et al., 2016; Peng et al., 2018; Tran et al., 2006; Weng et al., 2004; Yang et al., 2015; Yuan and Bauer, 2007; Zhang et al., 2014b; Zhou et al., 2014b). They can as well regulate the temporal variations of the SUHIs mainly over the inter- and intra-annual time scales (Fu and Weng, 2016; Lazzarini et al., 2015; Shen et al., 2016; Zhou et al., 2016a). Urban form can explain a substantial part of the pixel-by-pixel SUHI variations, via the factors related to the morphological properties (e.g., the area, compactness, and fractal dimension) of landscape patches within each city (Berger et al., 2017; Li et al., 2011; Yang et al., 2017; Zhou et al., 2011b); it can also control the city-by-city SUHI variations, via the factors related to the morphological properties of the entire city (e.g., the city size) (Clinton and Gong, 2013; Cui et al., 2016; Schwarz and Manceur, 2015; Zhang et al., 2012; Zhou et al., 2013, 2017). The temporal SUHI variations, especially at the inter-annual scale, would also be controlled partly by urban form (Ward et al., 2016). The anthropogenic heat generated by human activities is another substantial factor that impacts the SUHI variations at both the pixel and city scale (Liao et al., 2017; Wang et al., 2015; Yang et al., 2019); it is also able to impact the diurnal variations in the SUHIs (i.e., day-night contrasts), evidenced by its higher relationship with the nighttime SUHIs (Kato and Yamaguchi, 2005). Climate conditions also regulate the SUHI spatial variations over the regional/global scale and temporal variations over the inter- or intra-annual scales, through the interactions between land surface temperatures (LSTs) and some climatic variables (e.g. precipitation, humidity, wind, aerosols, and air temperatures) (Cao et al., 2016; Du et al., 2016; Peng et al., 2012; Yao et al., 2017; Zhao et al., 2014, 2018; Zhou et al., 2016b).

Analyses which integrate the controls of these aforementioned four groups of factors can generally capture the spatial variations of the SUHIs over all the scales from pixel to global, and also the associated temporal variations on the long-term (i.e., over the inter-annual time-scale) or mid-term (i.e., over the monthly/seasonal timescale) scales (Peng et al., 2012; Zhou et al., 2014a). However, it has been reported that SUHIs could also have large variations over the short-term scale (i. e., the day-to-day scale) mainly in response to specific daily weather conditions (He, 2018; Oke et al., 2017). For example, high wind speed tends to decrease the SUHI intensity (SUHII) and reduce the temperature variability, especially at night, by enhancing urban loss of sensible heat flux (through convection) and destroying (or preventing) rural surface based inversions that characterize strong rural cooling (Oke et al., 2017; Shaposhnikova, 2018). Clouds may dampen the SUHI due to their effects in blocking daytime incoming radiation and trapping nighttime long-wave radiation loss over both urban and rural surfaces (Oke et al., 2017). High humidity and precipitation would also weaken the SUHI, mainly by blocking the daytime solar radiation via the accompanied increase in cloud coverage, as well as by suppressing the nocturnal cooling especially over rural moist soils (Oke et al., 1991; He, 2018).

Previous studies have improved our understanding of SUHI controls by providing theories of the SUHI variations responsive to weather changes, whereas we still lack studies that can quantitatively affirm such responses using observations. While preliminary attempts have been made to quantify such responses (Shaposhnikova, 2018; Zhou et al., 2011a), these case studies have only focused on the impacts from a single or very limited meteorological variables on the SUHI intensity in a very small number of cities. As a result, there remain three unresolved fundamental questions related to the meteorological controls on the day-to-day SUHI variations: (1) For all the key meteorological variables that impact the SUHI and that are frequently observed (e.g., the relative humidity, wind speed, accumulated precipitation, and air temperature fluctuation), what is the rank (or relative importance) of their control on the SUHI variations? (2) Does the SUHI footprint (e.g., the area, shape,

and centroid which depicts the general spatial variations of the SUHI), like the SUHI intensity, vary significantly with weather changes? (3) Do the SUHI in cities within different climatic zones have different responses to the same weather variables? Without answers to these questions, our understanding of the controls of the day-to-day SUHI variations remains preliminary, therefore limiting our ability to predict and mitigate this phenomenon.

To address these issues, we characterized day-to-day variations in the intensity and footprint (including the extent, shape, inclination, and centroid) of nighttime SUHIs of 54 megacities in mainland China. Various meteorological variables obtained from in-situ measurements in these cities, which were anticipated to control the day-to-day variations in the SUHI, were incorporated as the main explanatory factors. Several variables determined to account for the mid-term components (i.e., the intra-annual variation) of SUHIs were also incorporated. It should be noted that the SUHI controls investigated in this study were restricted to nighttime conditions, mainly because of the considerably higher accuracies of satellite thermal observations during the night (see Section 5.3). This study is intended to help advance the understanding of SUHI controls on the day-to-day timescale.

2. Study area

China has experienced rapid urbanization in the past few decades (Zhao et al., 2015, 2015b), and a substantial SUHI effect has been reported for most cities (Zhou et al., 2014a). In this study, 83 major cities located in different bioclimatic zones were selected on the basis of criteria including urban size, urban population, the availability of at least one meteorological station within the administrative boundary, and administrative significance. At least one city was chosen from each province. For the selected megacities, nighttime SUHI features, including the intensity and footprint, were extracted from the daily LST images using a Gaussian model. Daily results deemed to be of poor quality were excluded from further analysis (see Section 3.2.1 for the quality evaluation methods). To ensure the reliability of the statistical analysis, we adopted the additional criterion that at least 50 daily SUHIs were incorporated in the correlations, and those cities with insufficient valid daily results were excluded. This resulted in a final total of 54 cities; their locations are shown in Fig. 1 and detailed information about them is given in Supplementary Information Table S1.

The cities are distributed within five bioclimatic zones: southern subtropical (SS), mid subtropical (MS), northern subtropical (NS), warm temperate (WT), and mid temperate (MT). Most of the selected cities were located in eastern China, which has a relatively flat terrain, mainly due to the high sensitivity of the Gaussian model to terrain. Both precipitation and temperature exhibit a decreasing trend from the southern to the northern cities (Fig. S1). For each city, all of the built-up pixels classified by the Climate Change Initiative (CCI) land cover product (see Section 3.1.1) were first identified. These pixels were then aggregated using an aggregation distance of 2 km as the urban area, following Zhou et al. (2014a). The rural area was then defined as the buffer zone outside the urban area (Bechtel, 2015; Cheval and Dumitrescu, 2009; Clinton and Gong, 2013; Debbage and Shepherd, 2015), with a radius of 15 km (Bechtel, 2015). In order to minimize the effects of water bodies and altitude within each city, all the pixels classified as water were removed, together with all the pixels with an elevation exceeding a certain threshold (defined as ±50 m of the median elevation over the built-up pixels) according to the Global 30 Arc-Second Elevation (GTOPO30) dataset. We defined the threshold according to the median rather than the averaged elevation in order to avoid the effects of fragmentary built-up pixels with extreme elevations.

3. Data and methods

3.1. Data

3.1.1. Satellite data

The satellite data used in this study include the land cover product in 2012 from the Climate Change Initiative (CCI) program of the European Space Agency (ESA) (ESA, 2015), as well as four categories of MODIS land product (collection 6) from 2012 to 2016: LST, AOD, normalized

Table 1
Information on the satellite data used in this study.

Data type	Product name	Spatial resolution	Temporal resolution
Land cover	CCI-LC	300 m	annual
LST	MYD11A1	1 km	daily
AOD	MCD19A2	1 km	daily
NDVI	MOD13A3/MYD13A3	1 km	monthly
albedo	MCD43C3	0.05°	16-day
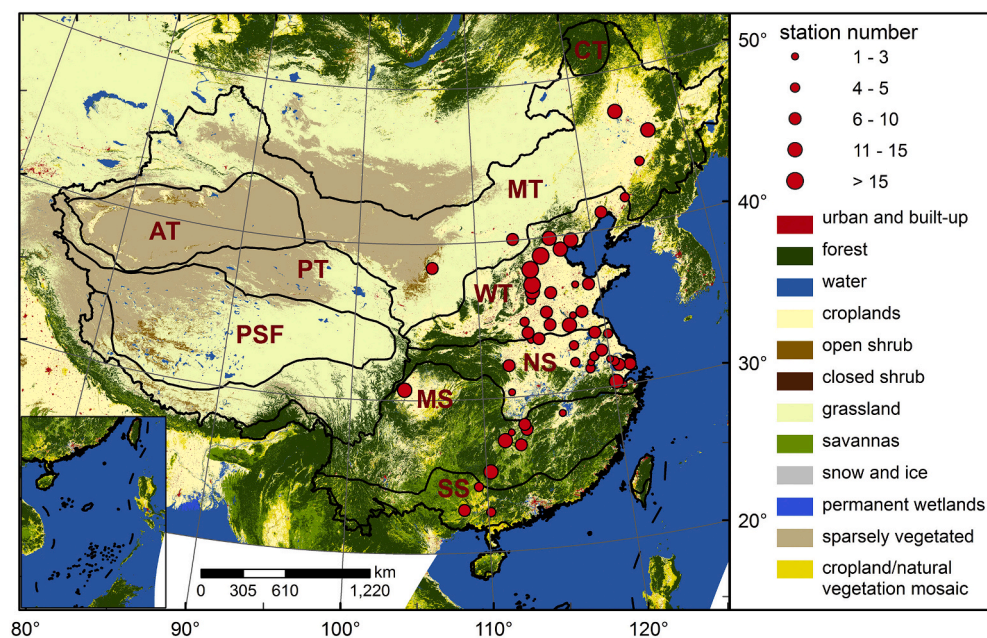
Fig. 1. Geolocation of the selected 54 megacities in China. The sizes of the red circles denote the number of meteorological stations within each city. The climatic zones are southern subtropical (SS), mid subtropical (MS), northern subtropical (NS), warm temperate (WT), mid temperate (MT), plateau temperate (PT), plateau subfrigid (PSF), arid temperate (AT), and cold temperate (CT). No cities in the CT, PSF, PT, and AT zones were chosen in this study. (For interpretation of the references to color in this figure legend, the reader is referred to the web version of this article.)

difference vegetation index (NDVI), and albedo (see Table 1). The land cover map has a spatial resolution of 300 m, which was further resampled to 1 km for consistency with the LST data, using a nearest neighbor resampling strategy. The LST data were derived from the daily nighttime MYD11A1 products (acquired at around 01:30) from the Aqua satellites, with a spatial resolution of 1 km. Retrieval errors of the MODIS LST data were claimed to be less than 1.0 K under most situations using the generalized split-window LST algorithm (Wan, 2008). To reduce the impact of cloud, all images with less than 50% valid urban or rural pixels were removed from the analysis (see Supplementary Information Fig. S2 for the cloud coverage for Chinese cities). The AOD data were derived from the daily MCD19A2 products, generated based on the new Multi-Angle Implementation of Atmospheric Correction (MAIAC) algorithm with a high accuracy (Lyapustin et al., 2018). The AOD at 550 nm, with a spatial resolution of 1 km, were used. The NDVI data were extracted from the monthly MOD13A3 and MYD13A3 products from the Terra and Aqua satellites, respectively. The associated spatial resolution is 1 km. The albedo data were obtained from the 16-day global MCD43C3 product with a spatial resolution of 0.05°, and the black sky albedo (BSA) in the shortwave band (0.3–5.0 μm) was used.

3.1.2. In-situ meteorological data

Daily weather conditions from 2012 to 2016 were collected from meteorological stations in the 54 Chinese megacities (see Fig. 1) from the China Meteorological Administration (CMA). Four major meteorological variables (the daily means of surface air temperature (SAT), wind speed, relative humidity, and daily accumulated precipitation) were used. The daily mean values of these variables are illustrated in Supplementary Information Fig. S1. Each of the datasets was subjected to a series of quality controls, including the assessment of climatic range, internal consistency, spatiotemporal consistency, and human-computer interaction (Ren et al., 2015). The daily accumulated precipitation data totals the amount measured during a 24-h period beginning at 20:00; days flagged as snowy were excluded from the precipitation dataset.

3.2. Methods

In order to comprehensively investigate the controls on nighttime SUHIs, quantitative indicators that are able to describe the overall spatial features of the SUHIs are required. Although it is usually straightforward to calculate the SUHI intensity (Voogt and Oke, 2003), the footprint of a SUHI, by comparison, is more difficult to quantify. The Gaussian model, one of the most widely used models for estimating the overall spatial features of nighttime SUHIs (Anniballe and Bonafoni, 2015; Quan et al., 2014; Zhou et al., 2011a), can simultaneously provide several parameters which together can be used to efficiently describe both the SUHI intensity and footprint (see Section 3.2.1 for more details) (Streutker, 2003; Tran et al., 2006). Moreover, its ability to derive SUHI features based on the LST spatial continuance generally makes it less susceptible to impacts from clouds. Therefore, we used the Gaussian model to parameterize the overall spatial features of the SUHIs. We acknowledge that the Gaussian model has certain limitations which may introduce biases into the SUHI quantification; this issue is discussed in Section 5.2.

The daily dynamics of the extracted nighttime SUHI features, as previously noted, are the combination of the SUHI mid-term variations (i.e., the annual/intra-annual variations) and day-to-day variations. These variations on different timescales are controlled by various groups of factors. Specifically, the annual averaged SUHIs within a city are controlled mainly by factors related to the urban form, anthropogenic heat release, and climatic conditions (Liao et al., 2017; Schwarz and Manceur, 2015; Zhao et al., 2014; Zhou et al., 2017). Intra-annual variations of the SUHIs are mainly controlled by factors related to land cover components and incoming radiation (Chen et al., 2006; Lazzarini et al., 2013). By contrast, weather conditions are suggested to be the dominant controls on day-to-day variations in SUHIs (Zhou et al.,

2011a). In this study, in order to investigate the controls on the daily SUHIs systematically, we decomposed the SUHI daily dynamics into two different timescales (the mid-term and day-to-day timescales, see Section 3.2.2 for more details). Two groups of variables related to the SUHI variations on these two timescales were incorporated as explanatory factors (see Section 3.2.3 for variable selection), and correlation analysis was used to examine their controls on the SUHIs (see Section 3.2.4).

3.2.1. Quantification of SUHI features

The Gaussian model was used to simulate nighttime LST images and to derive the daily SUHI features. The simulation consists of two stages (Streutker, 2003; Tran et al., 2006). In the first stage, the LSTs for the rural areas were fitted to a planar surface, and the SUHI signature was then derived by subtracting the rural temperature component from the LST image, based on Eq. (1):

$$
\begin{cases}
T_r(x, y) = T_0 + a_1 x + a_2 y \\
SUHI(x, y) = T_u(x, y) - T_r(x, y)
\end{cases}
\tag{1}
$$

where $T_r(x, y)$ is the nighttime LST for the rural pixel at location (x, y); T_0 is the rural mean surface temperature; a_1 and a_2 are the regression coefficients; $SUHI(x, y)$ is the SUHI signature for the urban pixel at location (x, y); and $T_u(x, y)$ is the nighttime LST for this urban pixel.

In the second stage, the extracted SUHI signature was fitted to a Gaussian surface, according to Eq. (2):

$$
\begin{cases}
SUHI(x, y) = a_0 \cdot exp(-U/2) \\
U = a_x^{-2} \cdot [(x - x_0)cos\varphi + (y - y_0)sin\varphi]^2 + a_y^{-2} \cdot [(y - y_0)cos\varphi - (x - x_0)sin\varphi]^2
\end{cases}
\tag{2}
$$

where a_0 is the height of the Gaussian surface; (x_0, y_0) is the location of the SUHI centroid; a_x and a_y are the half long axis and short axis of the Gaussian bottom ellipse, respectively; and φ is the inclination of the SUHI.

The Gaussian model provides a quantitative depiction of not only the SUHI intensity (i.e., the maximum magnitude represented by a_0), but also the extent (represented by a_x and a_y), shape (represented by the shape of the Gaussian ellipse), inclination (represented by φ), and centroid (represented by x_0 and y_0) of the SUHI. Five SUHI features were defined accordingly in order to describe the overall magnitude and spatial pattern of the SUHI (the definitions are given in Table 2); each feature has previously been used to quantify specific aspects of an SUHI (Anniballe et al., 2014; Quan et al., 2014; Schwarz et al., 2011; Streutker, 2003; Tran et al., 2006; Yang et al., 2019; Zhou et al., 2011a). In order to reduce the uncertainty caused by Gaussian modelling, the quality of each daily simulation was evaluated using the linear Pearson

Table 2
SUHI features derived from the Gaussian model.

SUHI feature	Physical basis	Variable	Description	Formula
Intensity	maximum SUHI magnitude	I	height of the Gaussian	a_0
Extent	area of the region most susceptible to the SUHI	A	area of the Gaussian ellipse	$\pi \cdot a_x \cdot a_y$
Shape	discrepancies in the SUHI in different directions	e	centrifuge rate of the Gaussian ellipse	$\sqrt{1 - a_x^{-2} \cdot a_y^2}$
Inclination	direction in which the SUHI is the most intensive	φ	inclination of the SUHI	φ
Centroid	location of the pixel with maximum SUHI magnitude	C_x	x coordinate of the SUHI centroid	x_0
		C_y	y coordinate of the SUHI centroid	y_0

correlation coefficient (r) and the root-mean-square error ($RMSE$) between the original LST image and the Gaussian-fitted LST image. Only fittings with r larger than 0.7 and $RMSE$ smaller than 1.5 K were regarded as valid for further analysis (the sensitivity of our results to this threshold is discussed in Section 5.2).

3.2.2. Temporal decomposition of daily SUHI features

The daily dynamics of the SUHI features listed in Table 2 can be decomposed into SUHI variations on the annual/intra-annual scale and those on the day-to-day scale. This is expressed as:

$$\lambda_{\mathrm{d}}(t) = \underbrace{\lambda_{\mathrm{a}} + \Delta\lambda_{\mathrm{a}}}_{\text{mid-term SUHI}} + \underbrace{\Delta\lambda_{\mathrm{d}}}_{\text{day-to-day variation}} = \lambda_{\mathrm{mid}} + \Delta\lambda_{\mathrm{d}} \qquad (3)$$

where $\lambda_{\mathrm{d}}(t)$ represents the daily value of SUHI feature λ on day t (i.e., the short-term SUHI); λ_{a} is the annual average of λ (i.e., the long-term SUHI); $\Delta\lambda_{\mathrm{a}}$ is the intra-annual variation of λ which, along with λ_{a}, represents the mid-term component of λ (i.e., λ_{mid}); and $\Delta\lambda_{\mathrm{d}}$ is the day-to-day variation of λ.

For each of the five SUHI features on a certain day, we quantified its mid-term component as the averaged value for a 15-day interval preceding and following that day, using Eq. (4):

$$\lambda_{\mathrm{mid}}(t) = N_{\mathrm{val}}^{-1}\left[\sum_{k=t-15}^{t-1}\lambda_{\mathrm{d}}(k) + \sum_{k=t+1}^{t+15}\lambda_{\mathrm{d}}(k)\right] \qquad (4)$$

where $\lambda_{\mathrm{mid}}(t)$ represents the mid-term component of SUHI feature λ on day t; N_{val} is the number of valid daily results during the 15-day interval either side of day t; and k represents the DOYs for the 15-day interval preceding and following the day t.

Here we selected the interval of 30 days considering that: (1) intra-annual variations are insignificant for this period close to one month, and (2) for most cases at least one valid result can be found within this 30-day interval - otherwise the result for that day must be excluded from further analysis because of the unavailability of mid-term SUHIs.

The day-to-day variations of each SUHI feature can thus be derived. For the SUHI features including intensity, extent, shape, and inclination, their day-to-day variations were calculated as the differences between their daily values and the computed mid-term components, according to Eq. (5):

$$\Delta\lambda_{\mathrm{d}}(t) = \lambda_{\mathrm{d}}(t) - \lambda_{\mathrm{mid}}(t) \qquad (5)$$

where $\Delta\lambda_{\mathrm{d}}(t)$ denotes the day-to-day variation of SUHI feature λ on day t; and $\lambda_{\mathrm{d}}(t)$ and $\lambda_{\mathrm{mid}}(t)$ are the same as in Eqs. (3) and (4).

For the SUHI centroid with two dimensions (i.e., C_{x} and C_{y}), two parameters were defined to quantify its day-to-day variations: the distance and the direction of the variations, which were calculated from Eq. (6):

$$\begin{cases} \Delta C_{\mathrm{dis\_d}}(t) = \sqrt{\left[C_{\mathrm{x\_d}}(t) - C_{\mathrm{x\_mid}}(t)\right]^2 + \left[C_{\mathrm{y\_d}}(t) - C_{\mathrm{y\_mid}}(t)\right]^2} \\ \Delta C_{\mathrm{dir\_d}}(t) = arctan\left\{\left[C_{\mathrm{x\_d}}(t) - C_{\mathrm{x\_mid}}(t)\right]^{-1}\cdot\left[C_{\mathrm{y\_d}}(t) - C_{\mathrm{y\_mid}}(t)\right]\right\} \end{cases} \qquad (6)$$

where $\Delta C_{\mathrm{dis\_d}}(t)$ and $\Delta C_{\mathrm{dir\_d}}(t)$ respectively represent the distance and direction of the day-to-day variation of the SUHI centroid on day t; $C_{\mathrm{x\_d}}(t)$ and $C_{\mathrm{y\_d}}(t)$ respectively represent the daily value of C_{x} and C_{y} on day t; and $C_{\mathrm{x\_mid}}(t)$ and $C_{\mathrm{y\_mid}}(t)$ correspondingly represent their mid-term components, as calculated using Eq. (4).

Noting that for 95% of the daily results, the distance of the day-to-day variation of the centroid is less than 8 km. This is reasonable since the SUHI centroid is closely related to the land cover status that is essentially constant over a short period (Quan et al., 2014). However, exceptions sometimes occur when the calculated centroid coordinates are more than 8 km away from the mid-term centroids. We consider such results less reliable and therefore they were excluded from further analysis.

After the temporal decomposition, the temporal dynamics over three different timescales (i.e., over the daily scale, mid-term scale and day-to-day scale) of each of the five SUHI features can be derived, which are listed in Table 3.

3.2.3. Selection of SUHI explanatory factors

The two decomposed components of the SUHI daily dynamics (λ_{mid} and $\Delta\lambda_{\mathrm{d}}$) were anticipated to have different controls. In order to comprehensively investigate the major controls on the daily SUHIs within each city, we incorporated various meteorological variables, which are hypothesized to be the controlling factors of $\Delta\lambda_{\mathrm{d}}$, as well as several factors related to λ_{mid} as the explanatory factors.

A total of 11 explanatory factors were included in the study, including 7 meteorological variables and 4 non-meteorological variables (see Table 4). Specifically, the meteorological variables selected were: the day-to-day variations of rural surface temperatures and SATs (termed $\Delta T_{\mathrm{r\_d}}$ and ΔSAT_{d}, decomposed from the daily dynamics of rural surface temperatures and SATs, based on Eqs. (4) and (5)); the daily mean values of wind speed, relative humidity, AOD, diurnal temperature range (DTR) of the rural LST; and the daily accumulated precipitation (WDS, RH, AOD, DTR_{r} and $PREP$). The variable DTR_{r} was employed to represent rural soil moisture: a higher DTR_{r} typically corresponds to a lower level of rural soil moisture (Oke et al., 2017). Only measurements on the days when valid quantification of SUHI was achievable were used. It should be noted that: (1) the quantification of the direct impact of precipitation on the SUHI is not achievable by remote sensing, mostly due to the unavailability of satellite observations during precipitation events. Nevertheless, considering the possible impact of antecedent precipitation on the SUHIs induced by the different water retention capacity in urban and rural surfaces after rainfall, we employed the daily accumulated precipitation ($PREP$) as a proxy of antecedent precipitation and analyzed its effect on the daily SUHIs. (2) For the surface and air temperatures, we employed their day-to-day variations in order to eliminate their substantial monthly/seasonal variations. However, for the other meteorological variables with less substantial seasonal variations but with large day-to-day variations, we directly employed their daily dynamics to avoid the uncertainty in calculating their day-to-day components. (3) All the meteorological variables, except those related to the background temperature and soil moisture ($\Delta T_{\mathrm{r\_d}}$ and DTR_{r}) were calculated based on all the available measurements within the administrative boundary of each city, in order to represent the meteorological conditions of the entire city.

The four non-meteorological factors which are related to mid-term variations of the SUHI features ($\Delta\lambda_{\mathrm{a}}$) (Chen et al., 2006; Zhou et al., 2011a) are: (1) the urban-rural contrast in vegetation status represented by the NDVI ($NDVI_{\mathrm{u-r}}$); (2) the albedo (ALB); (3) mid-term variation of the background surface temperatures (termed $T_{\mathrm{r\_mid}}$, decomposed from the daily dynamics of the rural surface temperatures based on Eq. (4)); and (4) the daytime length (DL, calculated according to Göttsche and Olesen (2009)). For the NDVI and albedo products with a temporal resolution coarser than 1 day, their daily values were designated using the observations on the most adjacent day. Finally, the background rural LST (T_{r}) was decomposed into two components: $T_{\mathrm{r\_mid}}$ as a non-meteorological factor, and $\Delta T_{\mathrm{r\_d}}$ as a meteorological factor.

Table 3
SUHI variables used to describe the variations of the SUHI features on different timescales.

Timescale	Variable	Description
Daily scale	I_{d}, A_{d}, e_{d}, φ_{d}, $C_{\mathrm{x\_d}}$, and $C_{\mathrm{y\_d}}$	daily dynamics of the SUHI features
Mid-term scale	I_{mid}, A_{mid}, e_{mid}, φ_{mid}, $C_{\mathrm{x\_mid}}$, and $C_{\mathrm{y\_mid}}$	the decomposed mid-term component of the SUHI features
Day-to-day scale	ΔI_{d}, ΔA_{d}, Δe_{d}, $\Delta\varphi_{\mathrm{d}}$, $\Delta C_{\mathrm{dis\_d}}$, and $\Delta C_{\mathrm{dir\_d}}$	the decomposed day-to-day component of the SUHI features

Table 4
Definition of the SUHI explanatory factors used for correlation analysis.

Factor	Description	Data source	Factor group[*]
ALB	albedo for each city	MODIS	A
$NDVI_{u\text{-}r}$	urban-rural contrast in NDVI	MODIS	A
T_{r_mid}	mid-term component of the daily rural LSTs	MODIS	A
DL	daytime length	calculation	A
ΔT_{r_d}	LST day-to-day variation across rural areas	MODIS	B
ΔSAT_d	SAT day-to-day variation	in-situ data	B
WDS	average wind speed for each city	in-situ data	B
RH	average relative humidity for each city	in-situ data	B
$PREP$	average precipitation amount for each city	in-situ data	B
AOD	average AOD for each city	MODIS	B
DTR_r	average DTR across rural areas	MODIS	B

[*] 'A' and 'B' indicate non-meteorological and meteorological factors, respectively.

3.2.4. Analysis of the relationship between SUHI features and explanatory factors

To explicitly investigate the controls of daily SUHIs, correlation analysis was conducted not only for the daily SUHIs, but also separately for the two temporal components of the SUHI daily dynamics (i.e., the mid-term and day-to-day components). The specific influence of antecedent precipitation on SUHIs was also derived via a comparison between the SUHI controls during periods with and without precipitation. Three scenarios of correlation analysis were consequently designed, each of which was conducted for each city (detailed information about the three scenarios is given in Table 5). For each correlation analysis, at least 30 pairs of variables were required to avoid statistical unreliability owing to small sample sizes (Maccallum et al., 1999).

3.2.4.1. Scenario #1: Controls on mid-term SUHIs and day-to-day SUHIs.
Controls on the mid-term SUHIs and on the day-to-day SUHIs were separately investigated for this scenario. The four non-meteorological variables (i.e., Group A in Table 4) were designated as the explanatory factors for the mid-term SUHIs; and the seven meteorological factors (i.e., Group B in Table 4) were designated as explanatory factors for the day-to-day SUHIs. The relationship between an explanatory factor and an SUHI variable was assessed using linear Pearson correlation analysis within each city. The associated explanatory power is evaluated by the correlation coefficient r and the associated significance p (a correlation is considered to be significant when p is less than 0.05). Noting that not all the SUHI features were included in the correlation analysis for this scenario. Specifically, the mid-term components of the SUHI centroid were excluded because this SUHI feature contains two dimensions (C_x and C_y), and as a result neither of them is able to represent the true dynamics of the SUHI centroid. In addition, the day-to-day variation of the SUHI inclination ($\Delta\varphi_d$) was also excluded because of its high sensitivity to uncertainties of the Gaussian fitting, especially for cities with a rotund SUHI ellipse.

Table 5
Information on the three scenarios used for correlation analysis.

Scenario	SUHI variables	Explanatory factor[*]	Correlation method
Scenarios #1 & #2	I_{mid}, A_{mid}, e_{mid}, and φ_{mid}	Group A	linear Pearson correlation
	ΔI_d, ΔA_d, Δe_d, ΔC_{dis_d}, and ΔC_{dir_d}	Group B	linear Pearson correlation
Scenario #3	I_d, A_d, e_d, and φ_d	Groups A + B (except $PREP$)	stepwise regression

[*] Here Groups A and B respectively denote the category of factors listed in Table 4.

3.2.4.2. Scenario #2: Comparison between the controls on mid-term SUHIs and day-to-day SUHIs during rainfall and non-rainfall periods.
The antecedent precipitation has been reported to potentially influence SUHI intensity as well as its sensitivity to other factors (Zhou et al., 2011a). In order to further investigate its effect on the SUHI features, including both the intensity and footprint, for various cities with different bioclimates, we compared the controls on the mid-term SUHIs and the day-to-day SUHIs during periods with and without antecedent precipitation. For each city, the daily samples were divided into two groups: periods with precipitation events occurring during the previous 72 h ('rainfall period'), and those without ('non-rainfall periods'). The numbers of daily samples classified in the 'rainfall period' and 'non-rainfall period' categories for each city are given in Table S1 in Supplementary Information.

3.2.4.3. Scenario #3: Controls on daily SUHIs.
By incorporating both the meteorological variables accounting for the day-to-day components of the SUHI daily dynamics and the non-meteorological variables accounting for their mid-term components, we further investigated the controls on the daily SUHIs within each city. To avoid multicollinearity, a stepwise regression analysis was employed to select the best variables in models for estimating the daily dynamics of SUHI features (including the intensity, extent, shape, and inclination). The variable $PREP$ was excluded from the stepwise regression because it is a constant (i.e., 0) on days with no precipitation. The thresholds of the p value for a variable to be added and removed were set as 0.05 and 0.10, respectively. For each model, the explanatory power was evaluated by the correlation coefficient r between the derived daily SUHIs and the true SUHI dynamics.

4. Results

4.1. Day-to-day variations in nighttime SUHI features

The nighttime SUHI features of the Chinese megacities were extracted using the Gaussian model. The associated simulation accuracy is illustrated in Fig. S3 given in Supplementary Information, which indicates that for most cities the mean r value of the Gaussian modelling exceeds 0.8 (Fig. S3b). The averaged magnitudes of the SUHI day-to-day variations are shown in Fig. 2. For most of the cities, the day-to-day variations of the intensity, extent, and shape of the SUHI respectively account for more than 20%, 25%, and 10% of their mid-term components (Fig. 2a–c). Although it may appear that these averaged annual percentages are not especially high, it should be emphasized that on specific days across the annual cycle, these three SUHI features can exhibit a day-to-day variation of more than 40%, 55%, and 30% of their associated mid-term components for nearly one-half of the cities, and the values are even higher for some cities. Also, the day-to-day trajectory of the SUHI centroid, when annually averaged, exceeds 0.6 km for all the cities (Fig. 2d); whereas on certain days across the annual cycle it can exceed 3 km for most cities.

To provide a better insight into the day-to-day variation in the SUHIs, we selected an individual city (Beijing) as an example. The daily dynamics of the SUHI features are illustrated in Fig. 3, wherein large day-to-day fluctuations in SUHI features are evident (Fig. 3ca1–a4). Furthermore, even during closely adjacent days when the land surface status was almost unchanged, the SUHI (both intensity and footprint) varied substantially (Fig. 3b1–b6). Specifically, within a period of less than 30 days, the SUHII can vary from 3.6 to 7.6 K; and the Gaussian-derived extent, shape, inclination, and centroid of the SUHI can exhibit great variations (Fig. 3c). We also found that such large day-to-day variations of the SUHIs are closely related to daily variations in weather conditions. For example, on a day with a relatively strong wind (e.g. DOY 090 with a wind speed of 3.6 m/s), the SUHI exhibits a small intensity and a biased central location compared to most other days (Fig. 3b6). This indicates the possible effect of wind in reducing the
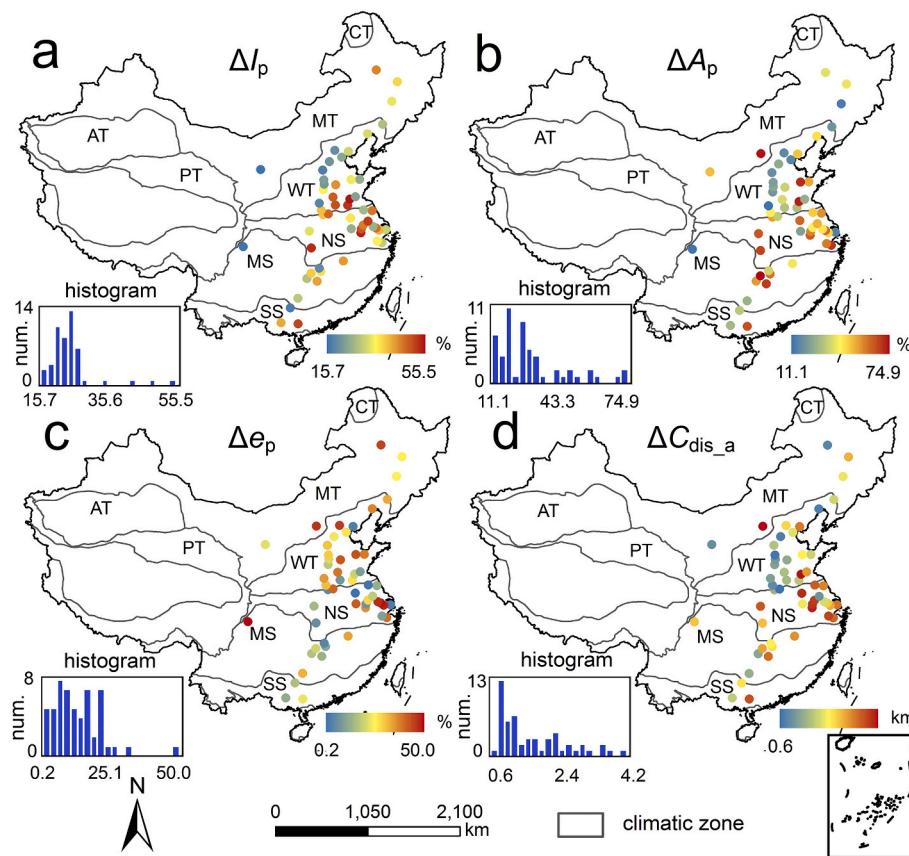
Fig. 2. Spatial distribution of the averaged magnitudes of the SUHI day-to-day variation. For the SUHI intensity, extent, and shape, the magnitudes (termed ΔI_p, ΔA_p and Δe_p, subplots a – c) were calculated as the averaged values of their day-to-day variations (i. e., ΔI_d, ΔA_d and Δe_d) normalized by their mid-term components (i.e., I_{mid}, A_{mid} and e_{mid}), according to Eq. (S1) in Supplementary Information. For the SUHI centroid, the magnitudes were directly calculated as the averaged values of the distance of its day-to-day variations (ΔC_{dis_d}).

intensity and changing the location of the SUHI (Oke et al., 2017). Precipitation can also alter the SUHIs. On a day when precipitation occurred (e.g. DOY 065), the nighttime SUHI exhibits a small intensity (3.6 K) accompanied by a large spatial extent (larger than 450 km^2) (Fig. 3b1). However, a large contrast, with a high SUHII (larger than 7.0 K) and a small SUHI extent (less than 350 km^2), is evident for the day following rainfall (e.g. DOY 084) (Fig. 3b5). The mechanisms responsible for this phenomenon may be variations in the surface moisture levels of impervious urban surfaces and rural soils during and after the precipitation events (He, 2018).

The results for Beijing demonstrate the occurrence of large day-to-day variations in SUHI features and the potential causal effect of weather conditions. However, quantitative investigations are needed to elucidate the meteorological controls on the SUHIs over more cities with different bioclimatic conditions.

### 4.2. Relationships between SUHI features and explanatory factors

4.2.1. Controls on mid-term SUHIs and day-to-day SUHIs

The correlation results for the mid-term components and day-to-day variations of daily SUHIs are illustrated in Figs. 4 and S4. For many of the cities, the mid-term dynamics of the SUHI features were controlled by the four non-meteorological variables. The other component of the daily SUHIs (i.e., their day-to-day variations), by comparison, are mainly regulated by weather conditions.

The greatest sensitivity to the weather conditions occurred for the SUHII (i.e. ΔI_d), with significant correlations with meteorological variables shown for most cities (Fig. S5). Among the meteorological variables, *RH* has the greatest influence (Figs. 4 and S4), which is understandable considering that on days with a higher *RH* value, more atmospheric water vapor would reduce the daytime radiation load at land surface, decrease the urban-rural difference in radiative cooling,

and therefore weaken nighttime SUHIs (Oke et al., 2017). The weakening effect from *RH* on the SUHI can also be explained by the reduced evaporative cooling especially for rural lands when the atmospheric water vapor pressure is higher. Similar SUHI weakening processes are responsible for the negative relationship between the *PREP* and SUHII, although the correlations between them are weaker (Fig. 4). A higher *PREP* value can also be related to a reduced SUHII through the suppressed nocturnal cooling of the rural moist soils when compared with that over the dry lands on days without antecedent precipitation (He, 2018). We are aware that the effect of *PREP* on SUHIs is delayed given the greater water retention capacity of rural soils than urban lands; further details are given in Section 4.2.2. Substantial effects of ΔT_{r_d}, *DTR*$_r$, and *AOD* on SUHII were also found for most cities. The effect of the former two variables can be attributed to their close correlations with background temperature, which greatly influence variations in SUHII. The effect of *AOD* on SUHII is also reasonable, as it can block incoming daytime shortwave radiation (Jin et al., 2010) while trapping longwave radiation at night, leading to a smaller urban-rural contrast in nocturnal radiative cooling rates and consequently weakening the nighttime SUHII. Notably, in contrast to the observed negative effect of *AOD* and *PREP* on the SUHII, several previous studies found positive correlations between these two variables and SUHIIs (Cao et al., 2016; Zhao et al., 2014). The seemingly contradictory results are likely due to the impacts from the scale on the SUHI controls (see Section 5 in Supplementary Information for further explanations).

The impacts of the other two meteorological variables related to atmospheric conditions (i.e., ΔSAT_d and *WDS*) on SUHII, by comparison, were less substantial. For example, the wind effect on the SUHII was only identified significant in a portion of cities where the winds are strong enough to profoundly reduce the LST through an intensified convective cooling. The less significant impacts of these two variables contrast with their dominant effects on CUHI intensity (CUHII)
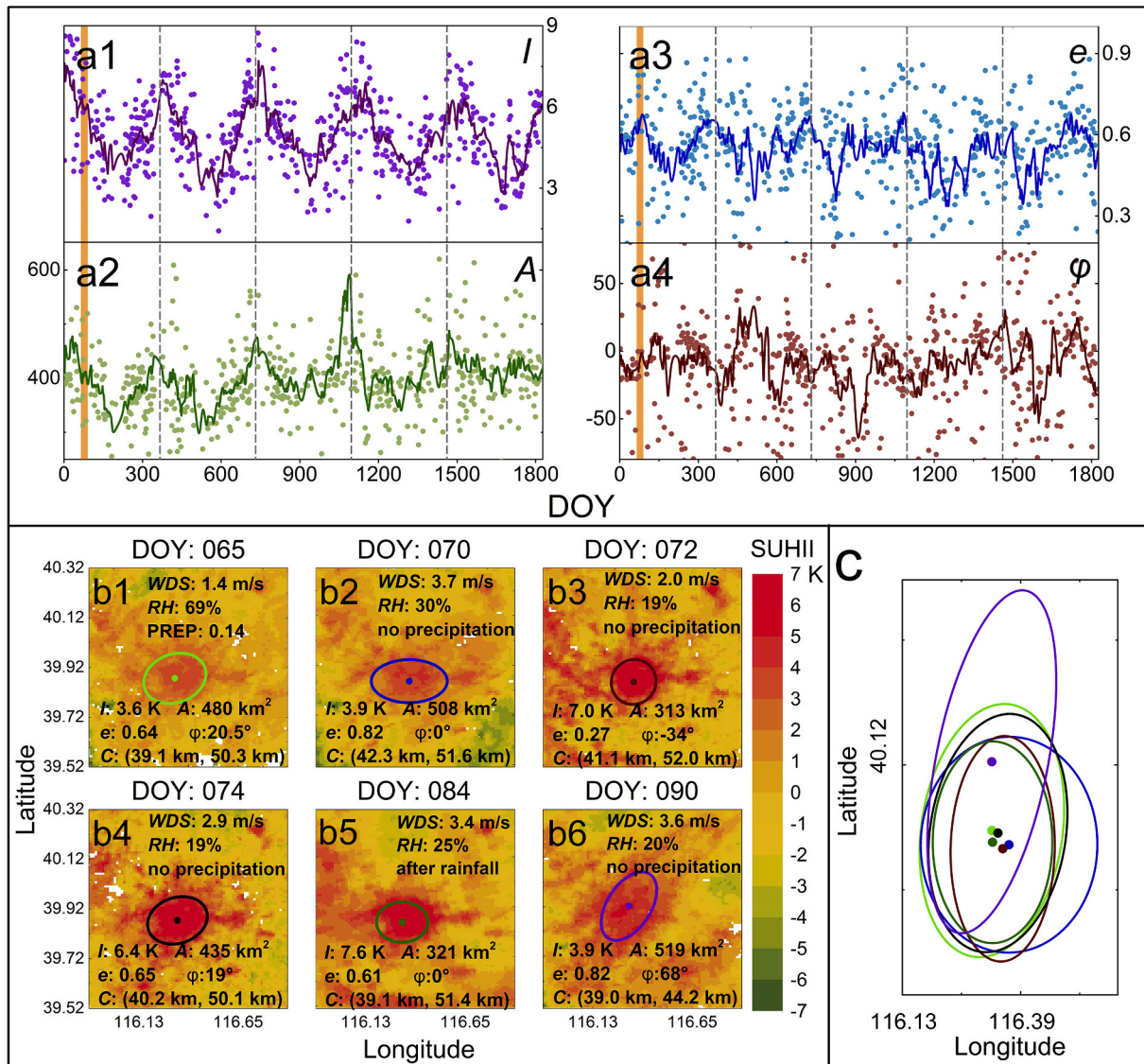
Fig. 3. Daily dynamics of nighttime SUHIs in Beijing. Subplots a1 – a4 illustrate the daily dynamics (dots) and mid-term variations (solid lines) of the four SUHI features (I, A, e, and φ) from 2012 to 2016, with the grey lines denoting the start (end) of each year. Subplots b1 – b6 illustrate examples of the fitted nighttime Gaussian-derived SUHIs for six days (within the orange bars in subplots a1 – a4), and subplot c compares these six Gaussian ellipses.

dynamics, especially for *WDS* (Oke et al., 2017). This suggests that, when compared with CUHII, SUHII is generally less sensitive to the factors related to atmospheric conditions.

The day-to-day variations of SUHI extent and shape (ΔA_d and Δe_d) are also less affected by the *WDS*. However, those variables that dominate the SUHI intensity (i.e., *RH*, *PREP*, *AOD*, and DTR_r) only exert significant influences on these two SUHI features in a small number of cities. Rather, they are more influenced by variables related to temperature fluctuations (i.e., ΔT_{r_d} and ΔSAT_d), suggesting the controls of background temperatures on SUHI footprint dynamics. Temperature fluctuations can also account for the day-to-day variation direction of the SUHI centroid (i.e., ΔC_{dir_d}). By contrast, for the variation distance of the SUHI centroid (i.e., ΔC_{dis_d}), the more dominant impact of *RH* and DTR_r was shown. Additional results show that the identified significant *WDS* impact on the SUHI centroid was shown only in parts of the cities characterized by relatively strong winds. This phenomenon, in contrast with the large impact of wind on the CUHI centroid, again indicates the lower sensitivity of the SUHIs to atmospheric motions.

The day-to-day variations of the SUHI footprint (i.e., ΔA_d, Δe_d, ΔC_{dis_d}, and ΔC_{dir_d}) are evidently less affected by weather conditions

than those of the SUHII. However, we consider that their actual dependences on weather conditions are likely underestimated in our results, mainly because of the uncertainty in terms of the Gaussian fitting (see Section 5.2 for more details). Despite this uncertainty, the major role of weather conditions was still identified for a number of cities.

4.2.2. Comparison of SUHI controls during periods of rainfall and non-rainfall

Precipitation has been identified as having a major influence on the SUHI features (Fig. 4). To further investigate the influence of precipitation, we made a detailed comparison of the SUHI characteristics during periods of rainfall and non-rainfall (Table S2 and Figs. 5 and 6). Evidently, precipitation events can reduce SUHIIs by ~0.5 K (Table S2), which is in accord with the results shown in Fig. 4.

It is also evident that antecedent precipitation may affect the sensitivity of the SUHI to other influencing factors (Figs. 5 and 6). For most of the SUHI features, the effect of the four non-meteorological variables is greater during rainfall periods than during non-rainfall periods. This suggests the occurrence of more significant intra-annual dynamics in the daily variations of the SUHIs during rainfall periods. The cause may be
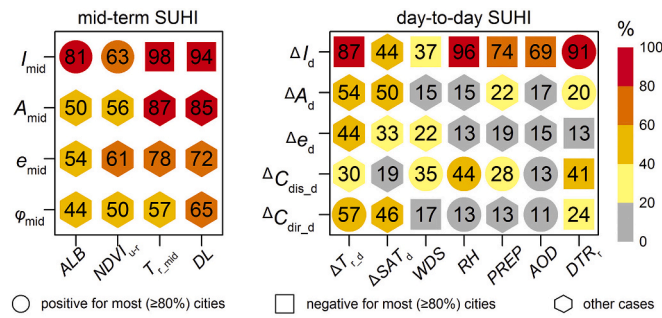
Fig. 4. Results of correlation analysis for mid-term SUHIs and day-to-day SUHIs. The numbers are percentages of megacities where there is a significant correlation (p is less than 0.05) between the associated SUHI variables and explanatory factors among all megacities. The circles (squares) denote that for most (more than 80%) of the cities where the associated SUHI variable and explanatory factor are significantly correlated, the correlations are positive (negative). Hexagons denote that the correlations among these cities show no consistency (i.e., neither positive nor negative). Further details about the correlation coefficients are given in Fig. S4.

Fig. 5. Results of correlation analysis for mid-term SUHIs and day-to-day SUHIs for periods of rainfall and non-rainfall. Symbols in this figure denote the same meanings as in Fig. 4.

related to a consistent effect of weather conditions on the SUHIs after precipitation events, e.g., the SUHIs always show a reduced intensity during rainfall periods (Fig. 4 and Table S2), and therefore the day-to-day variations of the SUHIs did not perturb the intra-annual dynamics of the SUHIs. The results further demonstrate a higher sensitivity of the SUHIIs to *RH*, *DTR*$_r$, and *AOD* during rainfall periods. Our assessment of the data leads us to infer that the larger ranges of variation of these three variables during rainfall periods enhance their correlations with the SUHII. By comparison, another meteorological variable, *WDS*, has a less significant impact on SUHI intensity and centroid during rainfall periods. The lower sensitivity to wind in rainfall periods is expected,

because variations of these two SUHI features in rainfall periods can be more strongly regulated by other variables which affect the radiative and evaporative cooling (e.g., *RH*, *DTR*$_r$, and *AOD*) while are consequently less sensitive to the wind which mainly affect the convective cooling.

4.2.3. Controls on daily SUHIs

Estimations of the daily SUHIs were obtained using the stepwise regression method, and the accuracies are given in Fig. S6. The explanatory power of the stepwise regression model, again, shows a higher contribution of meteorological variables in explaining the day-to-day variations in the SUHI intensity (the mean r value for the stepwise regression model is 0.72), when compared with those for the SUHI footprint (the mean r values are 0.37, 0.32, and 0.22 for the extent, shape, and inclination of the SUHI, respectively).

The specific controls of meteorological variables on the daily SUHI were analyzed by calculating the number of meteorological variables included in the stepwise regression model for each SUHI feature. The results (Fig. 7) again demonstrated a larger meteorological contribution to the SUHI intensity than to the SUHI footprint. Noting that there is one city in the MT zone where none of the meteorological variables were included in the regression model for the SUHII. This may be a result of the substantially more cloud cover as well as the poorer Gaussian-modelling performance in this city; these factors introduced uncertainties in the daily SUHI quantification (see further discussion in Section 5.2). Our results also indicate a minimal spatial difference in the meteorological controls on the SUHI extent, shape, and inclination over cities within different bioclimatic zones (Fig. 7b-d). For the SUHII, by comparison, a north-south contrast in meteorological controls is evident (Fig. 7a), with more meteorological variables included in the regression models in the northern temperate zones (i.e., the WT and MT zones) compared to the southern subtropical zones (i.e., the SS, MS, and NS zones).

In order to further investigate the meteorological controls on the daily SUHIIs, we counted the times that each meteorological variable was included in the stepwise model for each bioclimatic zone (Fig. 8). *RH* was revealed as the variable that contributes the most to the SUHII, followed by ΔT_{r_d} and *DTR*$_r$, in accordance with their identified significant correlations with the day-to-day SUHII variations in most cities (Fig. 4). *AOD* is also closely related to the day-to-day SUHII variations) (see Fig. 4), however, it has only a minimal impact on the daily SUHIIs when identified through a stepwise regression analysis. This small impact may be due to the high correlation between *AOD* and *RH*. Additional results demonstrated a similar zonal discrepancy for the two variables closely related to atmospheric conditions (ΔSAT_d and *WDS*): both have a higher contribution to the SUHII in northern cities (Fig. 8b–c). Such substantial zonal variations may sometimes lead to an underestimation of the effect of these two meteorological variables on daily SUHIIs. For example, *WDS* appears to have only a moderate effect on the SUHII when identified over all the cities in diverse climatic zones (Fig. 4). Nevertheless, the wind effect can be significant in some cities with specific climatic conditions (e.g. those within the WT zone) (Fig. 8b).
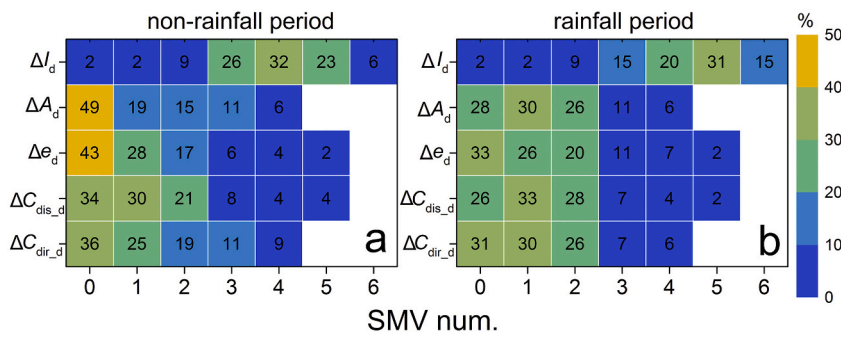
5. Discussion

By elaborating the meteorological effects on SUHIs, our results provide insights into the dominant controls on SUHI dynamics on the daily scale. The extracted day-to-day variations of the SUHIs highlight the occurrence of large deviations of daily SUHIs from mid-term SUHIs (see Figs. 2–3). The elucidated sensitivity of the SUHIs to weather conditions enhances our understanding of the SUHIs on days when the weather is not 'ideal'. More importantly, with the help of these predictable meteorological variables, our conclusions may provide a basis for the modelling and prediction of daily SUHIs. Several other issues relating to our results are discussed below.

Fig. 6. Numbers of significantly-related meteorological variables (SMV) for the SUHI day-to-day variations during non-rainfall periods versus those during rainfall periods. The x-axis represents the SMV numbers, and the y-axis represents the SUHI variables. For each square, the color and number denote the percentage of cities whose SMV number is equal to the x-axis divided by the total number of cities included in the associated correlation The variable 'PREP' was excluded from the analysis for both periods.
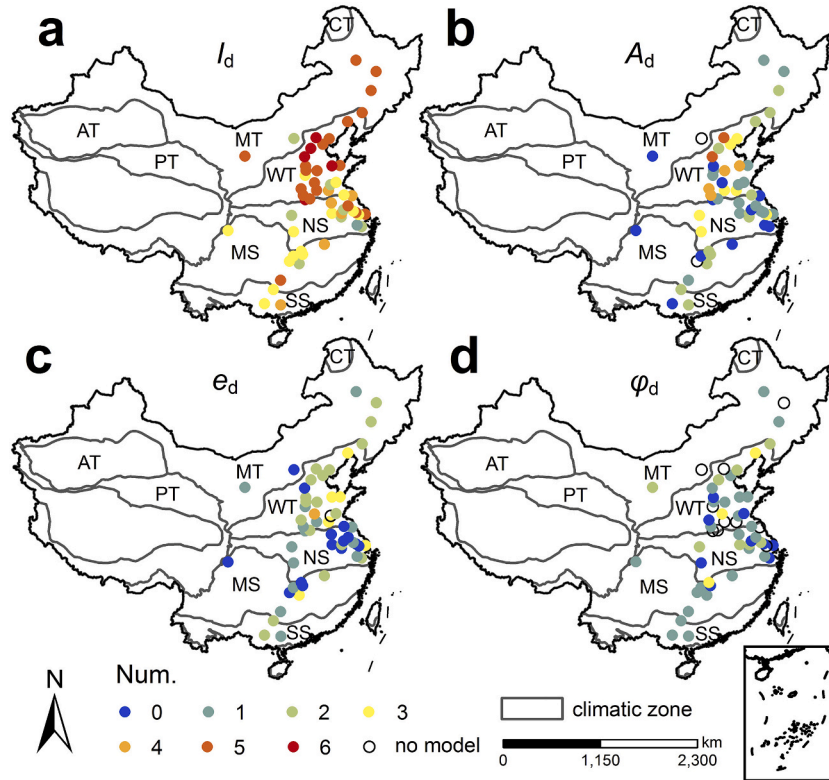
Fig. 7. Number of meteorological variables included in the stepwise regression model for SUHI intensity (I_d, subplot a), extent (A_d, subplot b), shape (e_d, subplot c), and inclination (φ_d, subplot d) over Chinese megacities.

## 5.1. Comparison of results to previous studies

Our study provides a big picture view of the controls of the day-to-day SUHI variations. The identified significant impacts from the four non-meteorological variables (including *ALB*, *NDVI*$_{u-r}$, *T*$_{r\_mid}$, and *DL*) on the mid-term SUHI variations correspond well to previous findings in terms of the dependence of the intra-annual SUHI variations on factors related to the land cover status or solar radiation (Peng et al., 2012; Wang et al., 2015; Zhou et al., 2014b). The notable impacts from *RH* on dampening the day-to-day SUHII, as well as the higher sensitivity of the SUHII to *AOD* and *RH* during rainfall periods, were also reported by previous studies (Oke et al., 1991; Oke et al., 2017; Zhou et al., 2011a). The phenomenon that wind can only substantially alter the SUHI when reaching a certain speed as well conforms to the observations by Allen (2017) and Shaposhnikova (2018).

Our results further reveal that the meteorological variables that account for the SUHI variations are sometimes different to those responsible for the CUHI variations. For example, the variable that contributes the most to the SUHII (i.e., *RH*) was shown less related to the CUHII (Oke

et al., 2017). Moreover, the meteorological variable that most affects the CUHIs (i.e., wind) (Arnds et al., 2017; Heaviside et al., 2014; Morris et al., 2001; Oke et al., 2017; Runnalls and Oke, 2000; Yow, 2007) only explains the SUHI variations in a portion of the cities. This contrast suggests the different physical mechanisms for these two layers of UHIs: The SUHI is relatively more sensitive to the surface thermal properties, while the CUHI is more dependent on the atmospheric transport, although these two UHIs are often closely related during the night (Nichol, 2005).

5.2. Possible uncertainties related to the data and methodology

The meteorological measurements used in this study were determined to have a high degree of accuracy after a series of quality control procedures (Ren et al., 2015). Their representativeness may still be affected by the relatively low density of meteorological stations, as well as the location and source area of stations, especially for those variables with a high spatial variability (e.g., wind speed). In addition, the disparity between the use of the daily mean values of meteorological
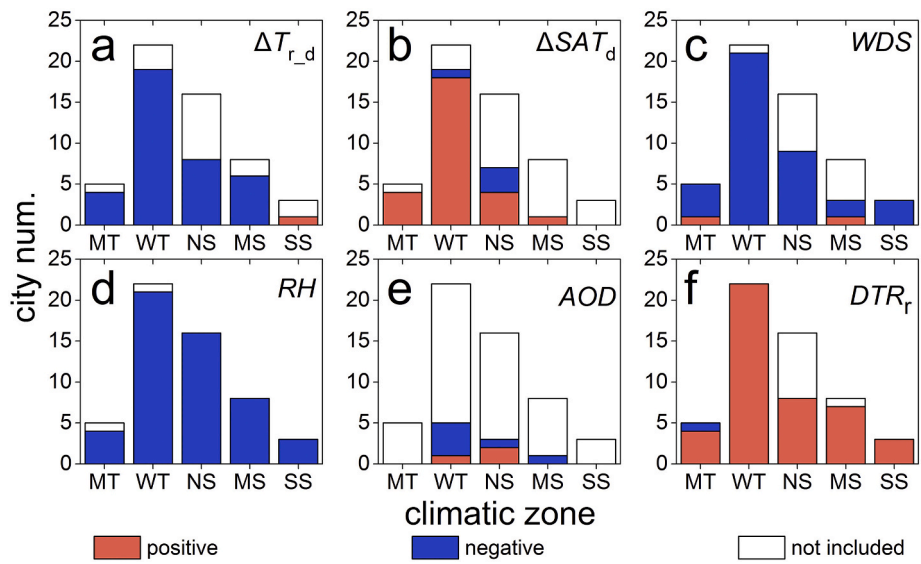
Fig. 8. Number of cities where each meteorological variable was included in the stepwise regression model for daily SUHI intensity, in each of the 5 Chinese climatic zones.

variables and the satellite nighttime observations obtained at instantaneous times may perturb the correlation analysis. Although our conclusions remain generally insensitive to this mismatch of the spatial/ temporal scales between the satellite and meteorological observations, such an uncertainty would still induce small biases to the SUHI-weather relationship (see Section 4 given in Supplementary Information). Future
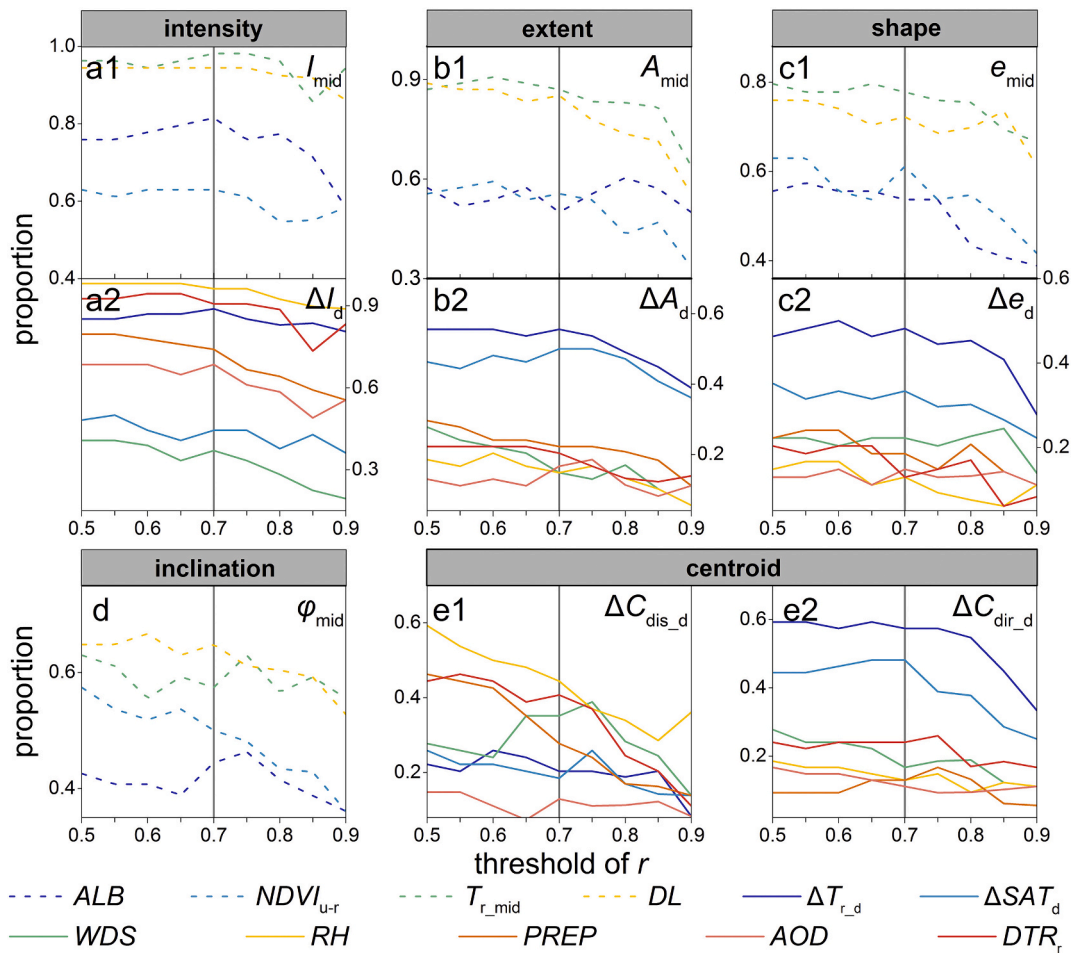
Fig. 9. Sensitivity of the correlation results to the Gaussian simulation performance. The x-axis denotes the threshold of *r* in the data preprocessing procedure which is set to range from 0.5 to 0.9 with an increment of 0.05, and the y-axis denotes the proportion of cities where the associated SUHI variable and explanatory factor are significantly related, accounting for the total number of cities included in the correlation. The grey lines correspond to the threshold of *r* adopted in this study (0.7).

studies may consider using instantaneous meteorological observations at the satellite overpass time, rather than the daily means, to better identify the sensitivity of the SUHI features to weather changes.

Biases may also be induced by the uncertainty of the MODIS LSTs, mainly in terms of thermal anisotropy and data gaps contaminated by clouds. Thermal anisotropy may sometimes decrease the LST accuracy, since satellites usually observe the land surface from different angles (Hu et al., 2016; Voogt, 2008). By employing nighttime data with a relatively weak anisotropic effect (Hu et al., 2016; Lagouarde and Irvine, 2008), this distortion was greatly reduced; nevertheless, biases may still exist, especially for pixels with a very slanted viewing angle. To further reduce the biases, future studies may perform angular normalization to adjust the slant LSTs into the nadir. By simulating the LST images using the Gaussian model based on the spatial continuity of the LSTs, our derived SUHI features may be less susceptible to the impact of data gaps. Noting that such data gaps may truly become a great concern during nights with substantial cloud cover (e.g. on nights when precipitation occurs), or within some southern cities with substantial missing data. A gap-filling strategy could be considered to derive gap-free images for these cities (Li et al., 2018). Another deficiency of satellite data that the LST data can only be obtained under clear-sky conditions hindered the investigation of the controls from another weather condition (i.e., cloud) on the daily SUHIs. A possible solution to this is to incorporate methods to derive cloudy-sky LSTs.

Uncertainty may also be introduced by the methodology, mainly by the incorporation of the Gaussian fitting and correlation analysis. The Gaussian model, despite its well-acknowledged efficiency in estimating the nighttime SUHI (Quan et al., 2014; Zhou et al., 2011a), may induce biased results. By removing the unsatisfactory modelled results using the data preprocessing procedure (see Section 3.2.1), we can maximize the accuracy of the remaining results. However, deviations still exist, particularly for the SUHI features related to the footprint. We therefore examined the sensitivity of the correlation results to the accuracy of the Gaussian fitting, and the results are displayed in Fig. 9.

The results show that when the r threshold is lower than 0.7, the correlation significance between each factor and the SUHIs typically remains stable along with the different degrees of Gaussian fitting performance. This suggests a low sensitivity of the overall correlation results to the Gaussian performance. We acknowledge that distortions may remain for some cities where the spatial pattern of the associated LSTs deviate from the Gaussian distribution (e.g., in some arid cities located in western China). A better model capable of accurately estimating the SUHI features is therefore required: e.g., an enhanced model that can better represent different types of urban thermal landscape. Further results show that when r exceeds 0.7, the correlation significance generally shows a decreasing trend along with the increase in r (Fig. 9). This is the result of the substantially smaller number of daily observations included in the correlation analysis once the threshold is set higher. We therefore consider 0.7 as a reasonable threshold of r, appropriate for the amount of data in this study, in order to reduce the uncertainties in terms of sample size. Nevertheless, we acknowledge that the sample-size issue may still be a concern for some SUHI features with a greater sensitivity (e.g., ΔC_{dis_d}, Fig. 9e1), especially in some southern cities with less valid daily results included in the correlation analysis (Fig. S3).

Uncertainties in terms of the correlation analysis mainly come from the selection of SUHI explanatory factors and the correlation strategy. To overcome the difficulty of obtaining large-scale observations of soil moisture with a high spatial resolution around urban surfaces, we employed the rural DTR (DTR_r) as a substitute. In spite of the close negative relationship between the DTR_r and soil moisture as revealed previously (Oke et al., 2017), we acknowledge that variations in the DTR_r are unable to accurately represent the variations in soil moisture because the DTR_r may also be responsive to other meteorological variables such as the humidity. Moreover, in spite of the identified dominant control from the meteorological variables that we selected in this study

(in Table 4) on the day-to-day SUHI variations, there still exist other factors that may, directly or indirectly, affect the day-to-day SUHIs. For example, factors related to the land cover and urban form may help modulate the variations of the SUHI (both its intensity and spatial patterns) in response to changes in weather conditions. As a result, SUHIs in cities or areas with different land cover components or urban forms may demonstrate different sensitivity towards weather changes. While in this study we only focused on the direct controls from meteorological variables on the SUHI variations, future studies may consider conducting additional analysis to investigate the effect from these other factors (e.g., land cover and urban form) on modulating the meteorological controls on SUHIs. In addition, the linear correlation strategy employed in this study may not be the best method to identify the SUHI controls, as the relationship between SUHI and the explanatory factors may not be linear. Future attention should be paid to developing a more efficient methodology to better identify the meteorological controls on daily variations of SUHIs (e.g., the support vector machine (SVM) regression model).

5.3. Rationale for studying the controls on nighttime rather than daytime SUHIs

The meteorological controls on the SUHIs elucidated in this study were restricted to the nighttime scenario. Controls for daytime SUHIs were not investigated, mainly because of the following inherent difficulties. First, strong thermal anisotropy exists for the daytime LSTs, which can lead to discrepancies of up to ~9.0 K for highly urbanized surfaces (Hu et al., 2016). Second, biases may also be affected more by the specific observation time in the day, during which the SUHIs exhibit large hourly variations (Lai et al., 2018b). Consequently, it is difficult to separate the day-to-day variations in SUHIs induced by differences in viewing angle and/or observation time from those induced by weather conditions. The 'thermal anisotropy' issue may be addressed by employing a model that can adjust the slant LSTs into the nadir; and the 'observation time' issue may be reduced by using data from geostationary satellites that provide continuous snapshots of the surface status at fixed times. Nevertheless, the complexity of the anisotropy correction algorithm and the deficiencies of geostationary data both restrict the investigation of the controls of daytime SUHIs on a continental/global scale. Another problem is the more frequent occurrence of data gaps due to clouds (Hu and Brunsell, 2013), as well as the additional difficulty in describing the overall spatial features of daytime SUHIs (Quan et al., 2014). A compromise solution to this problem, in cities with less cloud cover, may be to identify the controls on the SUHII only, which can be directly quantified (Voogt and Oke, 2003) without the Gaussian model.

Despite the difficulties in identifying synoptic controls for the daytime SUHIs, it is anticipated that daytime SUHIs will also demonstrate significant day-to-day variations in response to weather changes, although the sensitivity to each meteorological variable may show discrepancies from that for the nighttime one. For example, the impacts from the variable *AOD* on daytime SUHIs may be weaker than those on nighttime SUHIs (Cao et al., 2016).

6. Conclusions

Although the controls on SUHIs have been investigated intensively, the specific effects of weather conditions on SUHI variations on the daily scale have received less attention. In a study of megacities in China, we have extracted the day-to-day variations in SUHI features and correlated them with various meteorological variables. The results show that the intensity and footprint of SUHIs are highly variable, not only on the seasonal/annual scale but also on the day-to-day scale. We have identified significant meteorological controls on daily SUHIs and our specific findings are as follows.

The mid-term SUHI variations are substantially controlled by non-meteorological variables, while the day-to-day variations are mainly

regulated by meteorological variables. Among the various SUHI features, the SUHII is most sensitive to weather conditions. At least one meteorological variable is identified as a control on the SUHII for more than 90% of the cities, with the influence of ΔT_{r_d}, *RH*, *PREP*, DTR_r and *AOD* being the most important. The SUHI footprints (including the extent, shape, and centroid) are less but still significantly affected by weather conditions, whose dependence on each meteorological variable was identified within 10% to 60% of the cities. The SUHI extent, shape, and the variation direction of the SUHI centroid are impacted mainly by factors related to temperature fluctuations (i.e., ΔT_{r_d} and ΔSAT_d), whereas the variation distance of the SUHI centroid is more sensitive to *RH* and DTR_r. Further investigation determined that there are large differences in SUHI controls during periods with or without rainfall. Typically, during the rainfall period, the controls of *RH*, DTR_r, and *AOD* on the day-to-day SUHII variations were stronger, yet the wind impact was smaller. The results also demonstrate that the contributions from meteorological variables to the daily SUHII depend on the background bioclimate, which are considerably larger in cities in temperate zones than in subtropical zones. We acknowledge that the meteorological controls on SUHI features identified herein may be biased by uncertainties associated with the Gaussian fitting, and the conclusions are limited to nighttime. Nevertheless, we consider that our results contribute substantially to the understanding of the controls on SUHIs on the relatively poorly-investigated daily scale, and that they potentially provide a foundation for the modelling and prediction of the daily SUHI.

Declaration of Competing Interest

None.

Acknowledgments

Appendix A. Supplementary data

Supplementary data to this article can be found online at https://doi.org/10.1016/j.rse.2020.112198.

References

Akbari, H., Konopacki, S., 2005. Calculating energy-saving potentials of heat-island reduction strategies. Energ Policy 33 (6), 721–756. https://doi.org/10.1016/j.enpol.2003.10.001.

Allen, M.A., 2017. A method for hemispherical ground based remote sensing of urban surface temperatures. In: MSc. Thesis, Electronic Thesis and Dissertation Repository, 4594. Western University, Canada. http://ir.lib.uwo.ca/etd/4594.

Anniballe, R., Bonafoni, S., 2015. A stable Gaussian fitting procedure for the parameterization of remote sensed thermal images. Algorithms 8 (2), 82–91.

Anniballe, R., Bonafoni, S., Pichierri, M., 2014. Spatial and temporal trends of the surface and air heat island over Milan using MODIS data. Remote Sens. Environ. 150 (150), 163–171. https://doi.org/10.1016/j.rse.2014.05.005.

Arnds, D., Böhner, J., Bechtel, B., 2017. Spatio-temporal variance and meteorological drivers of the urban heat island in a European city. Theor. Appl. Climatol. 128 (1–2), 43–61.

Arnfield, A.J., 2003. Two decades of urban climate research: a review of turbulence, exchanges of energy and water, and the urban heat island. Int. J. Climatol. 23 (1), 1–26.

Bechtel, B., 2015. A new global climatology of annual land surface temperature. Remote Sens. 7 (3), 2850–2870. https://doi.org/10.3390/rs70302850.

Berger, C., Rosentreter, J., Voltersen, M., Baumgart, C., Schmullius, C., Hese, S., 2017. Spatio-temporal analysis of the relationship between 2D/3D urban site characteristics and land surface temperature. Remote Sens. Environ. 193, 225–243.

Cao, C., Lee, X., Liu, S., Schultz, N., Xiao, W., Zhang, M., Zhao, L., 2016. Urban heat islands in China enhanced by haze pollution. Nat. Commun. 7.

Chakraborty, T., Lee, X., 2019. A simplified urban-extent algorithm to characterize surface urban heat islands on a global scale and examine vegetation control on their spatiotemporal variability. Int. J. Appl. Earth Obs. 74, 269–280.

Chen, X.L., Zhao, H.M., Li, P.X., Yin, Z.Y., 2006. Remote sensing image-based analysis of the relationship between urban heat island and land use/cover changes. Remote Sens. Environ. 104 (2), 133–146.

Cheval, S., Dumitrescu, A., 2009. The July urban heat island of Bucharest as derived from MODIS images. Theor. Appl. Climatol. 96 (1–2), 145–153. https://doi.org/10.1007/s00704-008-0019-3.

Chow, W.T., Roth, M., 2006. Temporal dynamics of the urban heat island of Singapore. Int. J. Climatol. 26 (15), 2243–2260.

Clinton, N., Gong, P., 2013. MODIS detected surface urban heat islands and sinks: global locations and controls. Remote Sens. Environ. 134 (5), 294–304.

Cui, Y., Xu, X., Dong, J., Qin, Y., 2016. Influence of urbanization factors on surface urban heat island intensity: a comparison of countries at different developmental phases. Sustainability 8 (8), 706. https://doi.org/10.3390/su8080706.

Debbage, N., Shepherd, J.M., 2015. The urban heat island effect and city contiguity. Comput. Environ. Urban 54, 181–194. https://doi.org/10.1016/j.compenvurbsys.2015.08.002.

Deilami, K., Kamruzzaman, M., Liu, Y., 2018. Urban heat island effect: a systematic review of spatio-temporal factors, data, methods, and mitigation measures. Int. J. Appl. Earth Obs. 67, 30–42.

Du, H., Wang, D., Wang, Y., Zhao, X., Qin, F., Jiang, H., Cai, Y., 2016. Influences of land cover types, meteorological conditions, anthropogenic heat and urban area on surface urban heat island in the Yangtze River Delta urban agglomeration. Sci. Total Environ. 571, 461–470.

ESA-European Space Agency, 2015. Land Cover CCI Product User Guide Version 2.0. Available at: http://maps.elie.ucl.ac.be/CCI/viewer/download/ESACCI-LC-Ph2-PUGv2_2.0.pdf.

Fu, P., Weng, Q., 2016. A time series analysis of urbanization induced land use and land cover change and its impact on land surface temperature with Landsat imagery. Remote Sens. Environ. 175, 205–214.

Göttsche, F.M., Olesen, F.S., 2009. Modelling the effect of optical thickness on diurnal cycles of land surface temperature. Remote Sens. Environ. 113 (11), 2306–2316.

Haashemi, S., Weng, Q., Darvishi, A., Alavipanah, S., 2016. Seasonal variations of the surface urban heat island in a semi-arid city. Remote Sens. 8 (4), 352. https://doi.org/10.3390/rs8040352.

He, B.J., 2018. Potentials of meteorological characteristics and synoptic conditions to mitigate urban heat island effects. Urban Clim. 24, 26–33.

Heaviside, C., Cai, X., Vardoulakis, S., 2014. The effects of horizontal advection on the urban heat island in Birmingham and the west midlands, United Kingdom during a heatwave. Q. J. Roy. Meteor. Soc. 141 (689), 1429–1441.

Howard, L., 1833. The Climate of London, Vols. I–III, London.

Hu, L., Brunsell, N.A., 2013. The impact of temporal aggregation of land surface temperature data for surface urban heat island (SUHI) monitoring. Remote Sens. Environ. 134, 162–174. https://doi.org/10.1016/j.rse.2013.02.022.

Hu, L., Monaghan, A., Voogt, J.A., Barlage, M., 2016. A first satellite-based observational assessment of urban thermal anisotropy. Remote Sens. Environ. 181, 111–121. https://doi.org/10.1016/j.rse.2016.03.043.

Huang, F., Zhan, W., Voogt, J., Hu, L., Wang, Z., Quan, J., Ju, W., Guo, Z., 2016. Temporal upscaling of surface urban heat island by incorporating an annual temperature cycle model: a tale of two cities. Remote Sens. Environ. 186, 1–12.

Imhoff, M.L., Zhang, P., Wolfe, R.E., Bounoua, L., 2010. Remote sensing of the urban heat island effect across biomes in the continental USA. Remote Sens. Environ. 114 (3), 504–513. https://doi.org/10.1016/j.rse.2009.10.008.

Jin, M., Shepherd, J.M., Zheng, W., 2010. Urban surface temperature reduction via the urban aerosol direct effect: a remote sensing and WRF model sensitivity study. Adv. Meteorol. 2010 (2), 185–194.

Kato, S., Yamaguchi, Y., 2005. Analysis of urban heat-island effect using ASTER and ETM + data: separation of anthropogenic heat discharge and natural heat radiation from sensible heat flux. Remote Sens. Environ. 99 (1–2), 44–54.

Keramitsoglou, I., Kiranoudis, C.T., Ceriola, G., Weng, Q., Rajasekar, U., 2011. Identification and analysis of urban surface temperature patterns in greater Athens, Greece, using MODIS imagery. Remote Sens. Environ. 115 (12), 3080–3090. https://doi.org/10.1016/j.rse.2011.06.014.

Lagouarde, J.P., Irvine, M., 2008. Directional anisotropy in thermal infrared measurements over Toulouse city centre during the CAPITOUL measurement campaigns: first results. Meteorog. Atmos. Phys. 102 (3–4), 173. https://doi.org/10.1007/s00703-008-0325-4.

Lai, J., Zhan, W., Huang, F., Quan, J., Hu, L., Gao, L., Ju, W., 2018a. Does quality control matter? Surface urban heat island intensity variations estimated by satellite-derived land surface temperature products. ISPRS J. Photogramm. 139, 212–227.

Lai, J., Zhan, W., Huang, F., Voogt, J., Bechtel, B., Allen, M., Peng, S., Hong, F., Liu, Y., Du, P., 2018b. Identification of typical diurnal patterns for clear-sky climatology of surface urban heat islands. Remote Sens. Environ. 217, 203–220.

Lazzarini, M., Marpu, P.R., Ghedira, H., 2013. Temperature-land cover interactions: the inversion of urban heat island phenomenon in desert city areas. Remote Sens. Environ. 130 (4), 136–152.

Lazzarini, M., Molini, A., Marpu, P.R., Ouarda, T.B.M.J., Ghedira, H., 2015. Urban climate modifications in hot desert cities: the role of land cover, local climate, and seasonality. Geophys. Res. Lett. 42, 9980–9989. https://doi.org/10.1002/2015GL066534.

Li, J., Song, C., Cao, L., Zhu, F., Meng, X., Wu, J., 2011. Impacts of landscape structure on surface urban heat islands: a case study of Shanghai, China. Remote Sens. Environ. 115 (12), 3249–3263.

Li, X., Zhou, Y., Asrar, G.R., Zhu, Z., 2018. Creating a seamless 1 km resolution daily land surface temperature dataset for urban and surrounding areas in the conterminous United States. Remote Sens. Environ. 206, 84–97.

Liao, W., Liu, X., Wang, D., Sheng, Y., 2017. The impact of energy consumption on the surface urban heat island in China's 32 major cities. Remote Sens. 9 (3), 250.

Liu, W., Feddema, J., Hu, L., Zung, A., Brunsell, N., 2017. Seasonal and diurnal characteristics of land surface temperature and major explanatory factors in Harris County, Texas. Sustainability 9 (12), 2324. https://doi.org/10.3390/su9122324.

Lyapustin, A., Wang, Y., Korkin, S., Huang, D., 2018. MODIS collection 6 MAIAC algorithm. Atmos. Meas. Tech. 11, 5741–5765.

Maccallum, R.C., Widaman, K.F., Zhang, S., Hong, S., 1999. Sample size in factor analysis. Psychol. Methods 4 (1), 84–99.

Mathew, A., Khandelwal, S., Kaul, N., 2016. Spatial and temporal variations of urban heat island effect and the effect of percentage impervious surface area and elevation on land surface temperature: study of Chandigarh city, India. Sustain. Cities Soc. 26, 264–277.

Meng, Q., Zhang, L., Sun, Z., Meng, F., Wang, L., Sun, Y., 2018. Characterizing spatial and temporal trends of surface urban heat island effect in an urban main built-up area: a 12-year case study in Beijing, China. Remote Sens. Environ. 204, 826–837. https://doi.org/10.1016/j.rse.2017.09.019.

Morris, C.J.G., Simmonds, I., Plummer, N., 2001. Quantification of the influences of wind and cloud on the nocturnal urban heat island of a large city. J. Appl. Meteorol. 40 (2), 169–182.

Nichol, J.E., 2005. Remote sensing of urban heat islands by day and night. Photogramm. Eng. Rem. S. 71 (5), 613–621. https://doi.org/10.14358/PERS.71.5.613.

Oke, T.R., 1982. The energetic basis of the urban heat island. Q. J. Roy. Meteor. Soc. 108 (455), 1–24. https://doi.org/10.1002/qj.49710845502.

Oke, T.R., Johnson, G.T., Steyn, D.G., Watson, I.D., 1991. Simulation of surface urban heat islands under 'ideal' conditions at night. Part 2: diagnosis of causation. Bound.-Layer Meteorol. 56 (4), 339–358.

Oke, T.R., Mills, G., Christen, A., Voogt, J., 2017. Urban Climate. Cambridge University Press.

Patz, J.A., Campbell-Lendrum, D., Holloway, T., Foley, J.A., 2005. Impact of regional climate change on human health. Nature 438, 310–317. https://doi.org/10.1038/nature04188.

Peng, S., Piao, S., Ciais, P., Friedlingstein, P., Ottle, C., Breon, F.M., Nan, H., Zhou, L., Myneni, R.B., 2012. Surface urban heat island across 419 global big cities. Environ. Sci. Technol. 46 (2), 696–703. https://doi.org/10.1021/es2030438.

Peng, J., Jia, J., Liu, Y., Li, H., Wu, J., 2018. Seasonal contrast of the dominant factors for spatial distribution of land surface temperature in urban areas. Remote Sens. Environ. 215, 255–267.

Quan, J., Chen, Y., Zhan, W., Wang, J., Voogt, J., Wang, M., 2014. Multi-temporal trajectory of the urban heat island centroid in Beijing, China based on a Gaussian volume model. Remote Sens. Environ. 149 (7), 33–46.

Ren, Z., Zhang, Z., Sun, C., Liu, Y., Li, J., Ju, X., Zhao, Y., Li, Z., Zhang, W., Li, H., Zeng, H., Ren, X., Liu, Y., Zeng, X., 2015. Development of three-step quality control system of real time observation data from AWS in China. Meteorol. Monogr. 41, 1268–1277.

Runnalls, K.E., Oke, T.R., 2000. Dynamics and controls of the near-surface heat island of Vancouver, British Columbia. Phys. Geogr. 21 (4), 283–304.

Schwarz, N., Manceur, A.M., 2015. Analyzing the influence of urban forms on surface urban heat islands in Europe. J. Urban Plan. Develop. 141 (3), A4014003.

Schwarz, N., Lautenbach, S., Seppelt, R., 2011. Exploring indicators for quantifying surface urban heat islands of European cities with MODIS land surface temperatures. Remote Sens. Environ. 115 (12), 3175–3186. https://doi.org/10.1016/j.rse.2011.07.003.

Schwarz, N., Schlink, U., Franck, U., Großmann, K., 2012. Relationship of land surface and air temperatures and its implications for quantifying urban heat island indicators—An application for the city of Leipzig (Germany). Ecol. Indic. 18, 693–704.

Shaposhnikova, M., 2018. The Influence of Wind Speed on Night Time Surface Temperatures and the Surface Urban Heat Island of Phoenix AZ. MSc. Thesis. Western University, Canada.

Shen, H., Huang, L., Zhang, L., Wu, P., Zeng, C., 2016. Long-term and fine-scale satellite monitoring of the urban heat island effect by the fusion of multi-temporal and multi-sensor remote sensed data: a 26-year case study of the city of Wuhan in China. Remote Sens. Environ. 172, 109–125.

Sismanidis, P., Keramitsoglou, I., Kiranoudis, C.T., 2015. A satellite-based system for continuous monitoring of surface urban heat islands. Urban Clim. 14, 141–153. https://doi.org/10.1016/j.uclim.2015.06.001.

Stewart, I.D., Oke, T.R., 2012. Local climate zones for urban temperature studies. B. Am. Meteorol. Soc. 93 (12), 1879–1900. https://doi.org/10.1175/bams-d-11-00019.1.

Streutker, D.R., 2003. Satellite-measured growth of the urban heat island of Houston, Texas. Remote Sens. Environ. 85 (3), 282–289.

Tran, H., Uchihama, D., Ochi, S., Yasuoka, Y., 2006. Assessment with satellite data of the urban heat island effects in Asian mega cities. Int. J. Appl. Earth Obs. 8 (1), 34–48.

Tran, D.X., Pla, F., Latorre-Carmona, P., Myint, S.W., Caetano, M., Kieu, H.V., 2017. Characterizing the relationship between land use land cover change and land surface temperature. ISPRS J. Photogram. 124, 119–132.

Voogt, J.A., 2008. Assessment of an urban sensor view model for thermal anisotropy. Remote Sens. Environ. 112 (2), 482–495. https://doi.org/10.1016/j.rse.2007.05.013.

Voogt, J.A., Oke, T.R., 2003. Thermal remote sensing of urban climates. Remote Sens. Environ. 86 (3), 370–384. https://doi.org/10.1016/s0034-4257(03)00079-8.

Wan, Z., 2008. New refinements and validation of the MODIS land-surface temperature/emissivity products. Remote Sens. Environ. 112 (1), 59–74. https://doi.org/10.1016/j.rse.2006.06.026.

Wang, J., Huang, B., Fu, D., Atkinson, P., 2015. Spatiotemporal variation in surface urban heat island intensity and associated determinants across major Chinese cities. Remote Sens. 7 (4), 3670–3689.

Wang, K., Jiang, S., Wang, J., Zhou, C., Wang, X., Lee, X., 2017. Comparing the diurnal and seasonal variabilities of atmospheric and surface urban heat islands based on the Beijing urban meteorological network. J. Geophys. Res.-Atmos. 122 (4), 2131–2154.

Ward, K., Lauf, S., Kleinschmit, B., Endlicher, W., 2016. Heat waves and urban heat islands in Europe: a review of relevant drivers. Sci. Total Environ. 569–570, 527–539. https://doi.org/10.1016/j.scitotenv.2016.06.119.

Weng, Q., 2009. Thermal infrared remote sensing for urban climate and environmental studies: methods, applications, and trends. ISPRS J. Photogram. 64 (4), 335–344.

Weng, Q., Lu, D., Schubring, J., 2004. Estimation of land surface temperature–vegetation abundance relationship for urban heat island studies. Remote Sens. Environ. 89 (4), 467–483.

Yang, B., Meng, F., Ke, X., Ma, C., 2015. The impact analysis of water body landscape pattern on urban heat island: a case study of Wuhan City. Adv. Meteorol. 2015, 416728.

Yang, Q., Huang, X., Li, J., 2017. Assessing the relationship between surface urban heat islands and landscape patterns across climatic zones in China. Sci. Rep. 7 (1), 9337.

Yang, Q., Huang, X., Tang, Q., 2019. The footprint of urban heat island effect in 302 Chinese cities: temporal trends and associated factors. Sci. Total Environ. 655, 652–662.

Yao, R., Wang, L., Huang, X., Niu, Z., Liu, F., Wang, Q., 2017. Temporal trends of surface urban heat islands and associated determinants in major Chinese cities. Sci. Total Environ. 609, 742–754.

Yow, D.M., 2007. Urban heat islands: observations, impacts, and adaptation. Geogr. Compass 1 (6), 1227–1251.

Yuan, F., Bauer, M.E., 2007. Comparison of impervious surface area and normalized difference vegetation index as indicators of surface urban heat island effects in Landsat imagery. Remote Sens. Environ. 106 (3), 375–386. https://doi.org/10.1016/j.rse.2006.09.003.

Zhang, P., Imhoff, M.L., Bounoua, L., Wolfe, R.E., 2012. Exploring the influence of impervious surface density and shape on urban heat islands in the northeast United States using MODIS and Landsat. Can. J. Remote. Sens. 38 (4), 441–451.

Zhang, P., Bounoua, L., Imhoff, M.L., Wolfe, R.E., Thome, K., 2014a. Comparison of MODIS land surface temperature and air temperature over the continental USA meteorological stations. Can. J. Remote. Sens. 40 (2), 110–122.

Zhang, P., Imhoff, M.L., Wolfe, R.E., Bounoua, L., 2014b. Characterizing urban heat islands of global settlements using MODIS and nighttime lights products. Can. J. Remote. Sens. 36 (3), 185–196.

Zhao, L., Lee, X., Smith, R.B., Oleson, K., 2014. Strong contributions of local background climate to urban heat islands. Nature 511 (7508), 216–219.

Zhao, S., Zhou, D., Zhu, C., Qu, W., Zhao, J., Sun, Y., Dian, H., Wu, W., Liu, S., 2015. Rates and patterns of urban expansion in China's 32 major cities over the past three decades. Landsc. Ecol. 30 (8), 1541–1559.

Zhao, S., Zhou, D., Zhu, C., Sun, Y., Wu, W., Liu, S., 2015b. Spatial and temporal dimensions of urban expansion in China. Environ. Sci. Technol. 49 (16), 9600–9609.

Zhao, S., Zhou, D., Liu, S., 2016. Data concurrency is required for estimating urban heat island intensity. Environ. Pollut. 208, 118–124.

Zhao, L., Oppenheimer, M., Zhu, Q., Baldwin, J.W., Ebi, K.L., Bouzeid, E., Guan, K., Liu, X., 2018. Interactions between urban heat islands and heat waves. Environ. Res. Lett. 13 (3), 034003.

Zhou, J., Chen, Y.H., Wang, J.F., Zhan, W.F., 2011a. Maximum nighttime urban heat island (UHI) intensity simulation by integrating remotely sensed data and meteorological observations. IEEE J-STARS 4 (1), 138–146.

Zhou, W., Huang, G., Cadenasso, M.L., 2011b. Does spatial configuration matter? Understanding the effects of land cover pattern on land surface temperature in urban landscapes. Landsc. Urban Plan. 102 (1), 54–63.

Zhou, B., Rybski, D., Kropp, J.P., 2013. On the statistics of urban heat island intensity. Geophys. Res. Lett. 40 (20), 5486–5491.

Zhou, W., Qian, Y., Li, X., Li, W., Han, L., 2014a. Relationships between land cover and the surface urban heat island: seasonal variability and effects of spatial and thematic resolution of land cover data on predicting land surface temperatures. Landsc. Ecol. 29 (1), 153–167.

Zhou, D., Zhao, S., Liu, S., Zhang, L., Zhu, C., 2014b. Surface urban heat island in China's 32 major cities: spatial patterns and drivers. Remote Sens. Environ. 152, 51–61. https://doi.org/10.1016/j.rse.2014.05.017.

Zhou, D., Zhao, S., Zhang, L., Sun, G., Liu, Y., 2015. The footprint of urban heat island effect in China. Sci. Rep. 5, 11160.

Zhou, D., Zhang, L., Hao, L., Sun, G., Liu, Y., Zhu, C., 2016a. Spatiotemporal trends of urban heat island effect along the urban development intensity gradient in China. Sci. Total Environ. 544, 617–626.

Zhou, D., Zhang, L., Li, D., Huang, D., Zhu, C., 2016b. Climate-vegetation control on the diurnal and seasonal variations of surface urban heat islands in China. Environ. Res. Lett. 11 (7), 074009.

Zhou, B., Rybski, D., Kropp, J.P., 2017. The role of city size and urban form in the surface urban heat island. Sci. Rep. 7 (1), 4791.

Zhou, D., Xiao, J., Bonafoni, S., Berger, C., Deilami, K., Zhou, Y., Frolking, S., Yao, R., Qiao, Z., Sobrino, J., 2019. Satellite remote sensing of surface urban heat islands: Progress, challenges, and perspectives. Remote Sens. 11 (1), 48.